Journal of Innovations in Engineering Education
JIEE 2022, Vol. 5, Issue 1, pp 92-104.

https://doi.org/10.3126/jiee.v5i1.48052

THAPATHALI CAMPUS
Institute of Engineering
Tribhuvan University

Sediment erosion of head cover pressure balancing pipe-A Case study of Chameliya hydroelectric power station

Chiranjibi Acharya[a,*], Laxman Poudel[a,*] and Sudip Bhattrai[a,*]

[a]*Department of Mechanical and Aerospace Engineering, Pulchowk Campus, IOE, Tribhuvan University, Nepal*

ARTICLE INFO

Article history:

Received 04 Sep 2022
Received in revised form
14 Sep 2022
Accepted 15 Sep 2022

Keywords:

Chameliya Hydroelectric Power Station (CHEPS)
Computational Fluid Dynamics (CFD)
Discrete Phase Model (DPM)
Particle Size Distribution (PSD)
Finite volume method (FVM)
Pressure balancing pipe (PBP)
Elbow extrados/ intrados
Headcover

Abstract

The majority of rivers in the Himalayan basins have considerable concentrations of hard minerals (minerals with hardness greater than that of turbine material) in their sediment (minimum during the dry season and maximum during the wet season) causes to erode and deteriorate turbine parts. This deterioration causes frequent unit shutdowns for maintenance and repair, particularly during the wet season resulting in inconsistency in the generation of electrical power. In the case of the Francis turbine, one of the parts suffering from sediment-led erosion is the head cover and its pressure balancing pipe. The Chameliya Hydropower Plant (CHEPS), located in the Darchula district of Far-Western Province in Nepal has been used as a case study in this study to investigate the erosion caused by sediment in the head cover pressure balancing pipe which has been a significant erosion issue since commissioning. It is thus vital to foresee the erosion-prone locations in the balancing pipe in order to minimize the erosion thereby minimizing such losses. Analyses of erosion have been done by a field study at CHEPS and Computational Fluid Dynamics (CFD) based erosion modeling using a commercial CFD code ANSYS Fluent and the results were compared qualitatively and quantitatively. In the field study, eroded elbows were examined for erosion patterns, and lower elbow's (embedded with headcover having maximum erosion portion found by visual inspection) wall thickness was measured by cutting it into four lengthwise quarters. Additionally, the sediment concentration (ppm), PSD and Mineral content in the inflowing water was tested at Hydro Lab Pvt. Ltd., Lalitpur, Nepal by sampling the flow (incoming to the turbine) on various dates during the rainy season. The average concentration was found to be 2718.39 ppm, with the maximum concentration being 5308.70 ppm on July 4 and the minimum being 420.20 ppm on May 3. According to PSD analysis, 90% of the particles (by weight) fall in the range of 0.01 mm to 0.1 mm in the dry month and in the range of 0.01 mm to 0.5 mm in the wet month. Despite weather variations, the mineral composition of the silt was seen to be stable, with an average of 70.8% of the minerals being harder than the material of the pressure balance pipe (i.e. steel). Elbow wall thickness loss due to erosion was measured, and the erosion rate density at respective points was calculated. Using the average sediment concentration during the rainy season (2718.39 ppm) and the average particle size of 0.2 mm, erosion rate density was also calculated at the same locations using CFD simulation. The location of the erosion-prone area was the same as the real-life scenario, and the erosion rate density from the simulation follows the same trend as the experimental value with an deviation (average error) of 69.58%.

1. Introduction

The high concentrations of feldspar and quartz found in rivers, particularly in the Himalayan basins, have the potential to erode the turbine components of hydroelectric plants [1]. In the case of the Francis turbine, one of the parts suffering from sediment-led erosion is the head cover and its pressure balancing pipe. Pressure balancing pipe is located at the upper section of the Headcover and serves to relieve excessive water pressure leaking from the tip gap between the upper crown of the Francis runner and the inner circle of the Headcover. The leaking water has a high pressure and whirling motion, causing a massive upward thrust on the Headcover. To

*Corresponding author:
chiran.vsr@gmail.com (C. Acharya); laxman@ioe.edu.np (L. Poudel); sudip@ioe.edu.np (S. Bhattrai)

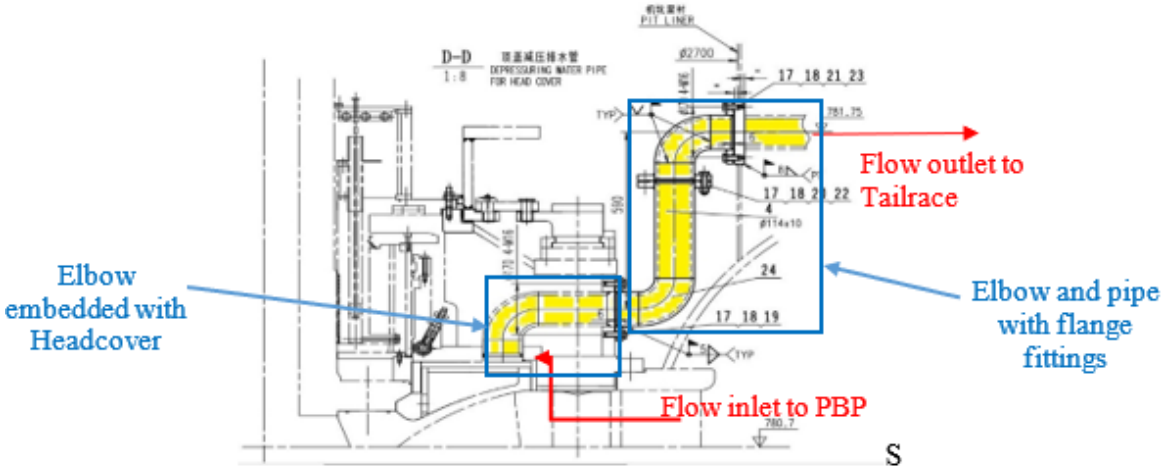

Figure 1: Headcover with Pressure balancing pipe (NEA, CHEPS)

reduce the force on the Headcover, a PBP is employed to relieve the leakage water's excessive pressure to Tailrace.

The Head Cover and its Pressure Balancing Pipe (PBP), a Francis turbine component, have been affected by significant silt erosion during the monsoon season, resulting in frequent unit shutdowns for maintenance and inconsistent energy generation. Since the Chameliya Hydroelectric Power Plant (CHEPS) was commissioned (February 10, 2018) sediment erosion in PBP has been a serious issue. So, a significant step should be taken to address this issue to some extent.

Sand's compositional minerals play a crucial role in characterizing it. Silica, quartz, mica, and feldspar are the most prevalent minerals in sand. Depending on its size, shape, mineral composition, texture, and hardness, sediment can be categorized into several types. The quantity varies depending on the source, the geology of the ground, chemical reactions, use, and additional factors like wind, water transformation, and weather [1]. The wear will increase with more sediment content and harder minerals like quartz and feldspar, which have higher hardness values, and this will cause the plant to function below its maximum capacity [2]. When the particles were large or micrometer-sized, as would be predicted, the erosion rate increased as the particle diameter grew. Similar reasoning applied to flow velocity, where faster flows aided in the erosion process. However, when the particle size shrank, the rate of degradation accelerated. This was explained by the secondary flows at the elbow, which centrifuged the particles toward the walls. The erosion rate for extremely small particles decreased once again when the particle distribution was pointed toward the pipe wall because their low mass was insufficient to erode the pipe wall [3]. Various particle sizes lead to various erosion patterns in the injection mechanism. Although the smaller particles may follow the streamlines and wear the needle tip abrasively, the larger particles had more inertia and were thus more likely to strike the upstream region of the needle orifice [4]. Particle impact velocity and bend radius may have a major influence on the rate and location of erosion [5].

Carbon steel 90° elbows are vulnerable to erosion-corrosion during multiphase flow, especially for abrasive slug flows. The results demonstrate that erosion-corrosion magnitude increases considerably as concentration levels grow. In comparison to the concentration of 2 weight percent sand fines in slug flow, the concentration of 10 weight percent sand fines in carrier phase increases the erosion-corrosion rate of carbon steel by up to 93% [6]. Erosion typically happens in the extrados of the pipe bend. The pipe bend type has an impact on the variations that have been observed, the increase in bend curvature directly correlates with an increase in erosion rate[7].

1.1. Problem statement

Since its commissioning, the CHEPS has been hampered by repeated unit shutdowns caused by significant Sediment erosion, which occurs primarily during the wet seasons. The problem is more pronounced in case of PBP. With wet season, the sediment loading in river increases, this causes the erosion of elbow, pipe and fittings of the PBP. As a result of this problem, the plant experiences significant energy loss due unit tripping, inconsistency in energy generation, which leads to an increase in the cost of repair and maintenance as well as

generation loss. Combined it is a significant economic loss for the plant. As a result, alternative methods should be employed to solve this challenge.

1.2. Objectives

1.2.1. Main Objective

To study the Sediment erosion on Head cover pressure balancing pipe of Chameliya Hydroelectric Power Station.

1.2.2. Specific Objectives

- To perform Qualitative and Quantitative analysis of Head cover pressure balancing pipe of CHEPS through field visit.
- To predict the Erosion pattern and Erosion rate density using ANSYS Fluent software.
- To compare the ANSYS simulation result (erosion rate density) with the result obtain from field measurement.
- To propose a design for erosion mitigation.

1.3. Limitations

- Cavitation's existence in the flow domain was neglected. Thus, the effect of the sediment particles will be the only cause of the mass loss.
- Since water is considered to be an incompressible fluid, there won't be any density changes. So ANSYS Fluent's pressure-based solver is assumed.
- The sediment concentration data of peak sediment containing month May 3rd, August 2nd was only considered.
- After colliding with a solid wall or another particle, the particles remain intact and do not degrade.
- Erosion-related geometry change is neglected.
- Corrosion effect is neglected

2. Methodology

2.1. Field visit/ measurement

A visit was conducted to the CHEPS in the Province No. 7 district of Darchula. During the visit the measurement was done on the following processes.

2.1.1. Qualitative measurement

The PBP's erosion was visualized, and at that time, a picture of the eroded elbow was taken. The snapshot collected allowed for the identification of the erosion-prone location.

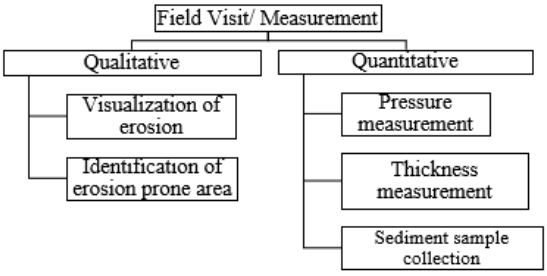

Figure 2: Procedure used for field measurement

2.1.2. Quantitative measurement

The dimension of existing PBP was measured. During the Unit's full load condition, the fluid pressure at the PBP's inlet and outlet sections was also measured through pressure gauge and found to be 0.15MPa and 0MPa respectively.

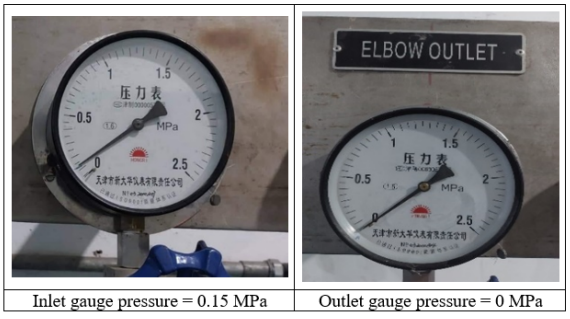

Figure 3: Pressure measurement

Only the lower elbow (elbow embedded with headcover) which was found excessively eroded through visual inspection during field visit was taken for thickness measurement. The thickness of the excessively eroded elbow (elbow embedded with headcover) was then measured using a Vernier caliper on several sections, and the loss thickness was taken into account for the study.

2.1.3. Thickness measurement

The Vernier caliper was employed to measure the elbow's thickness at various locations and loss of thickness at each location was calculated by using Equation 2. When measuring the thickness, the Vernier caliper's least count was 0.02mm. Uncertainty error also calculated by using Equation 1. Below is an explanation of the error analysis and loss of thickness calculation.

Error percentage in thickness

$$\sigma_t = \frac{LC}{t} \times 100 \tag{1}$$

where,
σ_t = percentage error in measurement of thickness
LC = least count of vernier caliper
t = thickness measured by vernier caliper

Loss of thickness calculation

$$\Delta t = \text{Design thicknesss} - t \tag{2}$$

where,
Design thickness = 10 mm

2.1.4. Erosion rate density calculation from field measurement

The erosion rate (where corrosion rate is neglected) in kg/m^2s was calculated by using the following formula [8].

$$\text{ERD} = \frac{\text{(Initial mass - Final mass)}}{\text{Impact Area} \times \text{Running time}} = \frac{m}{AT} \tag{3}$$

Where,
ERD = erosion rate density
m = eroded mass of wall material
A = Impact area of eroded portion
T = total erosion time

For small portion of erosion

$$\text{ERD} = \frac{\Delta m}{\Delta A \times T} = \frac{\rho \times \Delta t}{T} \tag{4}$$

where,
ρ = density of wall material
Δt = loss of thickness

After identification of loss of thickness, erosion rate density were calculated at different locations using the Equation 4 where the total erosion time (T) was used as 3 months of wet season.

2.1.5. Sediment sample collection

Sediment concentration (ppm), Particle size distribution and Mineral content in the inflowing water was tested at Hydro Lab Pvt. Ltd., Lalitpur, Nepal by sampling the flow (incoming to the turbine) on various dates during the rainy season. The results of sediment samples is mensioned in Appendix A, Appendix B & Appendix C.

2.2. Computational study for existing system

2.2.1. Geometry creation

The 2D drawing was created in CATIA V5 and then it was transferred into 3D. Here the dimensions are in millimeter and the elbows are short radius 90 ° elbow having 95 mm internal diameter with 10mm thickness, which has the radius of bend is same as its nominal diameter.

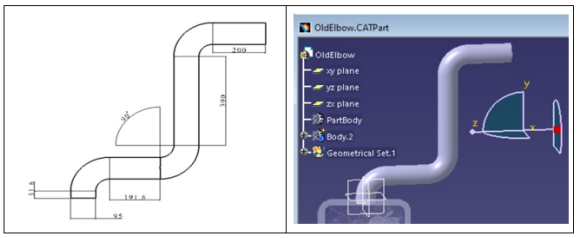

Figure 4: 2D and 3D CATIA drawing of existing PBP

2.2.2. Meshing

For mesh generation, the 3D geometry of an existing PBP was imported into ANSYS Fluent 21. The 3D domain as a whole was used to construct the mesh. To capture the impact of a sudden shift in flow direction, a fine mesh was utilized on the elbow with an O-grid tropology. Additionally, the 5 number of inflation layer was utilized close to the wall to capture the effects of the viscous layer (boundary layer) on fluid flow.

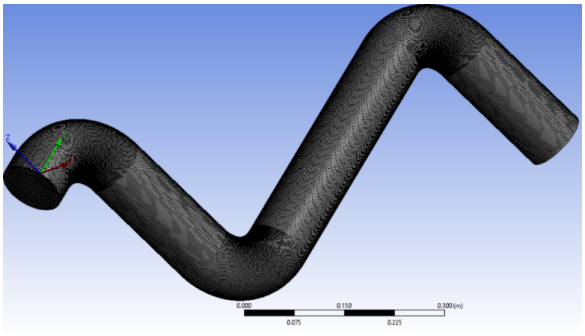

Figure 5: Meshing

2.2.3. Calculation of sand injection velocity

The velocity was calculated from the mass flow rate of water obtained from mesh independent test which was assumed to be sand injection velocity. The calculation details is shown in below.

$$\dot{m_w} = \rho_w \times A \times \vartheta \tag{5}$$

Where,
$\dot{m_w}$ = mass flow rate of water
ρ_w = density of water
A = cross section area of pipe inlet
ϑ = assumed velocity of sand particle

2.2.4. Calculation of total mass flow rate of sand

Utilizing the mass flow rate of water from the mesh independent test and the sediment content of the tested sample, the total mass flow rate of sand was computed.

The calculation details is shown below:

$$\dot{m}_s = \frac{\dot{m}_w}{\rho_w} \times PPM \times 10^{-3} \quad (6)$$

Where,
$\dot{m}_s$ = total mass flow rate of sand
$\dot{m}_w$ = mass flow rate of water
ρ_w = density of water
PPM = sediment concentration (parts per million)

2.2.5. Viscous Model (Turbulence model)

The viscous model made use of the Realizable k-ϵ model in ANSYS Fluent. Strong streamline curvature, vortices, and rotation are among the flow characteristics that distinguish it from the standard k-ϵ model. A modified transport equation for the dissipation rate, ϵ, was obtained from an accurate equation for the transport of the mean-square vorticity fluctuation and is included in the model as an alternate formulation for the turbulent viscosity. When a model is said to be "realizable," it indicates that it complies with specific mathematical restrictions on the Reynolds stresses that are in line with the physics of turbulent flow. Additionally, Standard wall function was employed for investigation of Near-wall treatment.

2.2.6. Erosion modelling

Generic Fluent, Finnie, McLaury, and Oka are the four erosion models that make up ANSYS Fluent in general. A model was developed out by B.S. McLaury to predict the erosion rate of sand particles in water [9]. On this study, the McLaury erosion model was preferred. The McLaury erosion rate is determined by

$$E = AV^n f(\gamma); \quad A = FBh^k \quad (7)$$

where,
F = Empirical Constant,
V = Particle impact velocity,
B_h = Brinell's hardness number of wall material,
k is a constant that depends on material composing wall.

For erosion analysis in ANSYS Fluent, discrete phase model (DPM) was used for sand particle injection. Sand particle was used as inert particle type and with surface injection. Diameter distribution was taken as uniform with the value, 0.2 mm, that was obtained from PSD curve of sediment sample. The velocity magnitude was taken as 11 m/s which was obtained from mass flow rate from mesh independent test. Additionally, the sediment concentration of the sample was used to calculate the total mass flow rate of sand by using Equation 6. The maximum erosion rates were identified at different sediment concentration and then compared with the calculated erosion rate density from field measurement.

2.2.7. Boundary conditions

In ANSYS Fluent, the flow simulation was carried out. Drawing, field measurement, and ANSYS CFD analysis were used to collect all the required data. The findings so acquired were examined in the ANSYS Fluent post to observe the required erosion rate density, pressure distribution, and velocity distribution. Table 1 below displays the details of parameters and boundary conditions utilized during the erosion simulation.

Table 1: Parameters and boundary conditions for erosion simulation

Analysis Type	Pressure based, Steady state
Fluid and Particle	Water and Quartz
Inlet/ Outlet condition	
Gauge total pressure inlet/ outlet	150000 Pa, 0 Pa
Direction	Normal to boundary
Turbulent intensity	5%
Turbulent viscosity ratio	10
Discrete phase type	escape
Wall condition	
Wall motion	Stationary wall
Shear condition	No slip
Roughness	Standard
Discrete phase type	Reflect
Erosion Analysis	
Erosion model	McLaury erosion model
Average diameter of Quartz	0.2mm
Viscous model	Realizable k-ϵ, standard wall function (Turbulence intensity = 5%)
Injection velocity of Quartz	11 m/s
Injection type	Surface, inject using face normal direction
Mass flow rate of Quartz	0.2120 kg/s
Density of Quartz	2650 kg/m3
Wall material	Steel (density = 8030 kg/m3)
Pressure-velocity coupling	SIMPLE method
Spatial discretization	Least square based, PRESTO
Number of iteration	1000
Convergence criterion	0.001 residual

2.2.8. Result validation

The result obtained through the computational analysis and filed measurement was compared. The validation of the result was done by comparing the location of erosion prone area (from photograph) and erosion rate density at different locations.

3. Results and discussions

3.1. Results of CFD Simulation

3.1.1. Mesh independence

The mesh independent test was performed by using the inlet, outlet pressure readings from field measurement (0.15Mpa, 0 MPa). Mesh size influences boundary

Table 2: Mesh independent test

Number of elements	Mass flow rate (kg/s)	Percentage of error
(M5) 3489500	75.12	
(M4) 1644184	77.12	2.7%
(M3) 1015372	77.84	0.9%
(M2) 562500	89.53	15.0%
(M1) 277875	125.19	39.8%

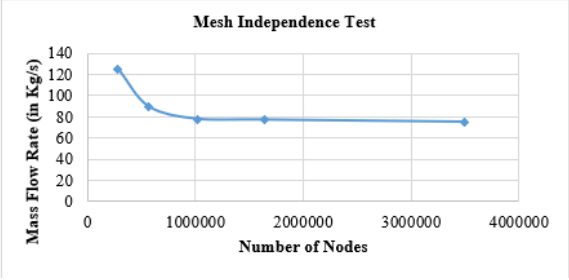

Figure 6: Mesh independence

layer refinement control in a direct proportion. The desired value (mass flow rate) varies from 277875 (M1) to 3489500 (M5) for the various element numbers, and mass flow rate was taken into consideration as the parameter of interest during the test. Figure 6's graph of the mesh independent test shows that the value of mass flow rate does not significantly change after a fine mesh of 1015372 (M3) elements. As a result, the M3 mesh set M3 (1015372 elements) was chosen from the mesh independence test to lower the computational cost and time taking into account the resources available. Further computational analysis of erosion rate also employed the equivalent mass flow rate value of 77.84 kg/s. Equation 5 was used to compute the inlet velocity, which was used to represent the velocity of sand injection.

3.1.2. Pressure contours

Figure 7 represents the pressure distribution in PBP. From visualizing the figure, the pressure goes on decreasing almost smoothly along the center line of pipe moving from inlet to outlet but it is not as smooth along the wall surface where the pipe bends occur. Due to the sudden change in flow direction the pressure at bend extrados (outer curvature) was found higher than intrados (inner curvature). Here Zone 1 shows the high pressure region and Zone 2 shows the low pressure region (even negative pressure region).

3.1.3. Velocity contours

The velocity distribution in the PBP is shown in Figure 8 With almost zero velocity occurred at the surface certain ahead of intrados (Zone 3) while moving from inlet to

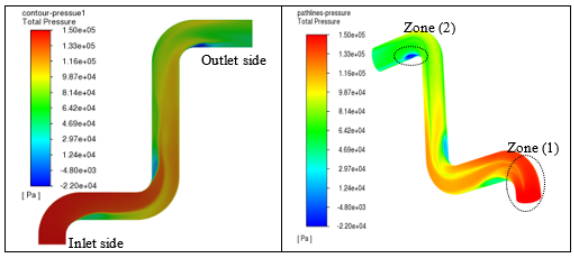

Figure 7: Pressure distribution in PBP

exit whereas the velocity at the bend intrados was found to be high.

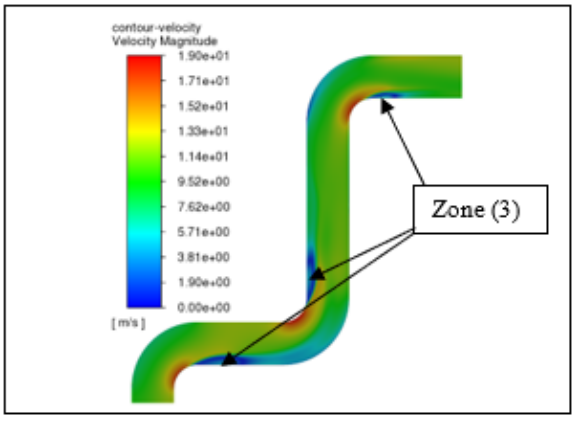

Figure 8: Velocity distribution in PBP

3.2. Sediment sample results

3.2.1. Dry weight of suspended sediment sample

Sediment samples were collected from draft tube side of CHEPS during the monsoon season (2021 May to August), when pipe failure due to erosion is most common, the concentration of sediment was measured. Each sample was collected in one liter of sediment led water, and the dry weight were measured after that sediment concentration was calculated (ppm). Figure 9 shows the concentration of sediment from May 3 to August 2. Sediment concentration was found rising from 420.20ppm (May 3) to 4262.30ppm (June 13) , then slightly decreasing to 4045.50ppm on June 23 and then rising again to a maximum of 5030.70 on July 4 and decreasing up to 2056.10ppm on August 2. The rise in concentration could be the result of high flood and construction activities (Hydropower construction, Road construction etc.). Over the course of the time, the average concentration was found to be 2718.39 ppm. Sediment concentration results from Hydro Lab Pvt. Ltd. is shown in Appendix A.

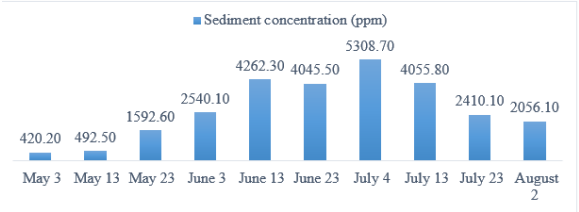

Figure 9: Concentration of sediment from May 3 to August 2

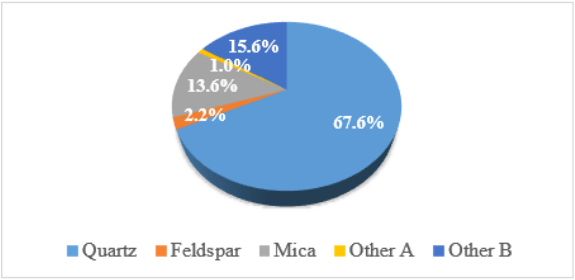

Figure 10: Pie chart of mineral content analysis

3.2.2. Particle size distribution (PSD)

Around 90% of the particles in BS 2078 Fagun (February 2022) (dry month) are under the range (0.01 to 0.1) mm whereas during same year of Shrawan (2021 August) (wet month) particle size are under the range (0.01 to 0.02) mm. However, the majority of the particles in the recent year BS 2079 Jestha, Ashad, and Shrawan (2022 June, July and August) rainy season were found to be in the range of (0.01 to 0.5) mm. The PSD graph shows that throughout the monsoon season, 80% of the sand particles have been flowing. Due to the flood rising in rainy season, particle size and sediment concentration may both rise. Human activities such as construction of a hydroelectric plant and the construction of roads in the upstream region may be responsible for larger particle size flowing this year compared to previous year. Results of PSD from Hydro Lab Pvt. Ltd. is shown in Appendix B.

3.2.3. Mineral content

According to the analysis of the sediment sample, the sample contains quartz, feldspar, mica, tourmaline, garnet, hornblende, olivine, and clay. The most prevalent of them is quartz, which is present in around 67.6% of it. Despite weather variations, the mineral composition of the silt was seen to be stable on different months, with an average of 70.8% of the minerals being harder than the material of the PBP (i.e. cast steel). The principal hard minerals identified thus far include quartz, feldspar, garnet, and tourmaline. Figure 10 shows the pie chart of mineral content analysis. Results of Mineral content from Hydro Lab Pvt. Ltd. is shown in Appendix C.

Other A : Tourmaline, Garnet, Hornblende and Olivine

Other B : Carbonate (14%), Clay, Organic matters, and upto 2% unidentified mineral and rock fragments (slate)

3.3. Field Investigation of Eroded Elbow

3.3.1. Photographs

At the time of the field visit, the erosion in the PBP could be visually represented. The lower side elbow extrados area experienced excessive erosion. The Unit has repeatedly been shut down for the repair (repair by welding) of the leaking region because of the excessive erosion, mostly during the rainy season.

Elbow that was dismantled during overhauling period was cut into different sections and visualized and measured the thickness. Observing the erosion pattern as shown in Figure 11 (b), the rate of erosion rises as one moves from the inlet (the bottom part) to the outlet (the upper portion). The outer curvature of the bend was found to have excessive erosion, holes, but the inner curvature had less erosion than the outer curvature which is shown in Figure 11 (a).

Figure 11: Erosion in elbow

3.3.2. Thickness measurement at different positions

The Vernier caliper having least count 0.02 mm was employed to measure the elbow's thickness (excessively eroded elbow embedded with headcover). The thickness was measured in different sections; side wall section (A, A', B, B', C, C', D, D', E, E',F, F', G, G', H, H', I, I') and Outer curvature section (1', 2', 3', 4', 5', 6', 7', 8', 9'), total 27 sections, in order to compute the loss of thickness due to erosion. The loss of thickness was calculated by subtracting the measured thickness from design thickness (10 mm). Figure 12 shows the different positions for thickness measurement.

Loss of thickness at different positions were calculated by using Equation 2 and percentage of uncertainty er-

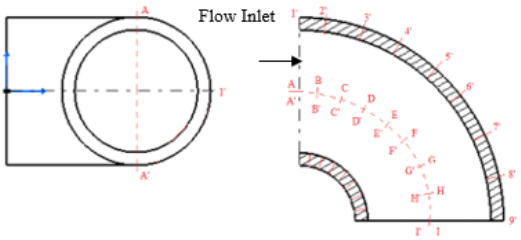

Figure 12: Different positions for thickness measurement

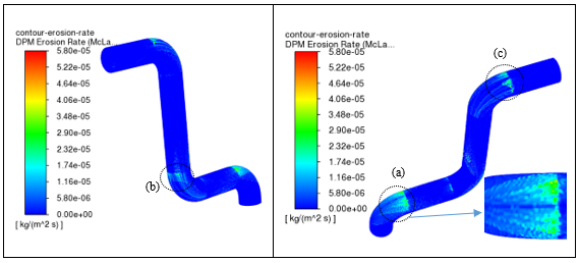

Figure 13: Erosion rate density contour

ror during thickness measurement were calculated by using Equation 1. The average loss of thickness and uncertainty error was found to be 5.54mm and 0.76% respectively.

3.3.3. Erosion rate density calculation

Erosion rate density at different locations (as shown in Figure 12 were calculated by using the Equation 4. For the purpose of calculating erosion rate density, the total erosion time (T) was assumed to be 3 months. After identification of erosion rate density at different locations, locations 5', 6', 7', 8', 9', F, G, H, I, F', G', H' and I' were found to be the most eroded places, while the average erosion rate density was determined to be 5.71714E-06 kg/m$^2 s$.

3.4. CFD modeling of Erosion

Sand mass flow rates during the wet season were calculated by using the Equation 6, and the resulting data were utilized to compute erosion rate density. The total mass flow rate of sand corresponding to the average sediment concentration (2718.39 ppm) was found to be 0.2120 which was used to compute the erosion rate density at different locations.

3.4.1. Erosion prone area

Figure 13 shows different locations where the PBP wall has experienced erosion. The average sediment concentration during the wet season was used to calculate the erosion rate density in ANSYS Fluent 21, McLaury model of erosion. The elbows' outside curvature (a, b, and c) was found to be more risk to erosion than other areas. Among the three elbows, the lower side elbow area (a) was found as the erosion prone area. So, the field measurement was done mainly on the lower side elbow.

3.4.2. Erosion at different sediment concentration

Samples taken during the wet season (2021 May to August), when pipe failure due to erosion has been most common, the concentration of sediment was measured from Hydro Lab Pvt. Ltd, Lalitpur. The different measured values of sediment concentration were used to observe the erosion rate density.

According to Figure 14 erosion rate rises in response to rising sediment concentrations and vice versa. The leakage from the balance pipe caused by sediment erosion will thus probably happen more frequently during the rainy season when sediment flow is at its highest. It would be concluded that, sediment concentration is one of the primary factors causing erosion on material surfaces.

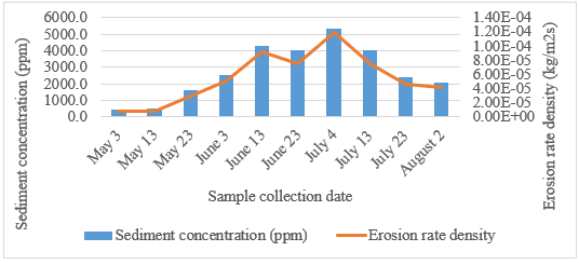

Figure 14: Erosion rate density at Sediment concentration

3.4.3. Erosion rate density at different locations

Erosion rate density at different locations (as shown in Figure 12 were also computed from simulation by using average sediment concentration of wet season (2718.39 ppm) and quartz diameter 0.2mm. Figure 2.10, 2.11 & 2.12 show the graph of erosion rate density at different locations where locations 6', 7', 8', 9', F, G, H, I, F', G', H' and I' were found to be the most eroded places, while the average erosion rate density was determined to be 1.01199E-05kg/$m^2 s$.

3.5. Comparison of Results

3.5.1. Qualitative comparison

In the qualitative comparison, the erosion-prone area was identified by photographing the running elbow and

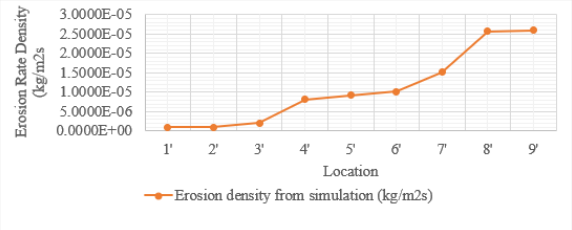

Figure 15: Erosion rate density at outer curvature (1' to 9')

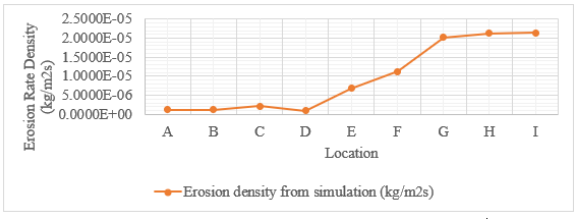

Figure 16: Erosion rate density at outer front wall (A to I)

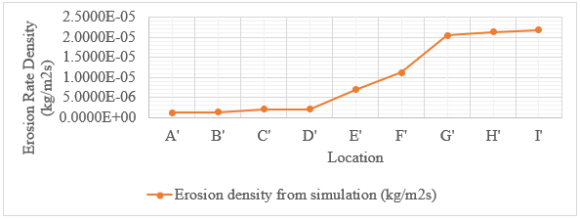

Figure 17: Erosion rate density at outer front wall (A' to I')

the disassembled deteriorated elbow during the overhauling period. The erosion at the extrados of the lower side elbow was found to be excessive due to the high pressure and direct impact on the surface, as illustrated in Figure 11. The results from simulation also indicated that the erosion-prone region was found at the extrados of lower side elbow, as illustrated in Figure 13. In comparison, According to simulation and experiment results, the position of the erosion-prone area was found to be identical.

3.5.2. Quantitative comparison

The erosion rate density calculated from field measurement using 3 months (wet season) of erosion running time and loss of wall thickness and was compared with the value of erosion rate density from ANSYS Fluent simulation using average sediment concentration of 3 months (wet season). Following Figures show the comparison of simulation and experiment results on different locations (outer radius of curvature; 1' to 9', frontside wall; A to I, and backside wall; A' to I') of elbow. It was

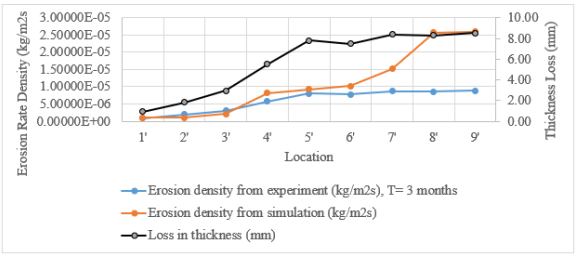

Figure 18: Graph of erosion rate density and thickness loss on outer curvature

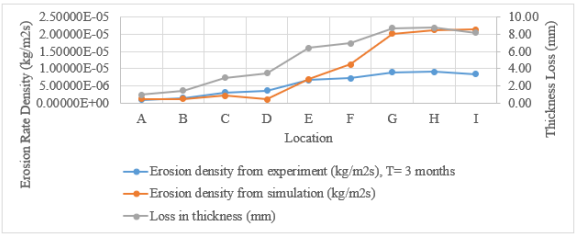

Figure 19: Graph of erosion rate density and thickness loss on frontside wall surface

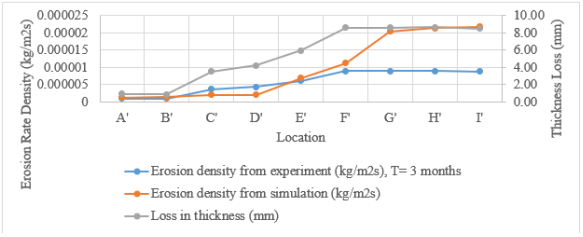

Figure 20: Graph of erosion rate density and thickness loss on backside wall surface

discovered from all three comparisons (Figure 18, 19, & 20) that the erosion rate rises when moving from inlet to exit, albeit marginally decreasing in a few spots. The zone of outer curvature (4' to 9') and both side walls (E E' to I I') were found to be erosion prone area which is also shown in Figure 21. In addition, erosion rate density

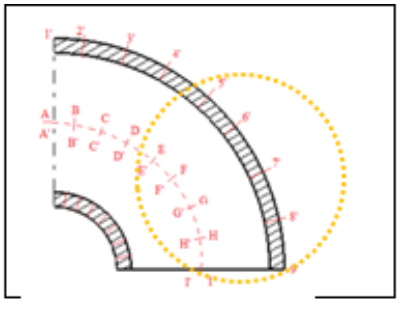

Figure 21: Location of erosion prone area

obtained from simulation exhibits the same pattern as the actual value, with an average difference of 69.58 percent. This discrepancy may have been brought about by measurement-related instrumentation errors, discretization mistakes connected to the numerical technique for solving equations, and flow-normalization assumptions made during numerical modeling.

4. Conclusion

(i) To identify the erosion-prone area, pictures of the running elbow and the damaged elbow that had been disassembled were taken during the field visit. It was found that there was significant erosion at the lower side elbow extrados. In order to model erosion using CFD, the average sediment concentration (2718.39 ppm) and sediment size (0.2 mm diameter) from sediment sampling were determined. Measurement of the elbow wall thickness after three months of installation and subtraction with original thickness was done for the calculation of thickness loss in various elbow parts. A field visit also showed that the leaks in the balancing pipes were discovered more frequently in the wet season. In conclusion, sediment concentration is one of the major factors causing erosion on material surfaces.

(ii) The Mclaury erosion model was then used for CFD-based erosion modeling. After modeling the sample concentration, and average sediment size, and conducting the simulation, it was revealed that the same location of maximum thickness loss found during the field visit had a high erosion rate density and area of erosion. In conclusion, modeling and experiment data closely matched each other, revealing an erosion-prone zone. It was also seen from CFD that the erosion rate density increases in response to increasing sediment concentrations and vice versa after simulations with various sediment concentrations from testing samples were done. Sediment particles directly affect the elbow's outside curvature as the flow rapidly switches from the intake to the outlet. As a result, without consideration of cavitation effect it was found that the sediment erosion is greatest on the surface of outer curvature while the cavitation may occur on the inner curvature due to the negative pressure developed (Zone 2) which is shown in Figure 7

(iii) The erosion rate density at differnet locations (as shown in Figure 12) from the simulation follows the same trend as the experimental results with an deviation (average error) of 69.58%.

5. Recommendations

(i) For more accurate comparison of the erosion, it would be recommended to use digital image processing for calculating the erosion rate density

(ii) After erosion, the flow regime in the wall shifts, resulting in an area of high local velocity and correspondingly low pressure, which starts the cavitation process. To precisely understand the beginning of cavitation in Pressure balancing pipe, more research using CFD models and tests is advised.

References

[1] Poudel L, Thapa B, Shrestha B P, et al. Computational and experimental study of effects of sediment shape on erosion of hydraulic turbines[J/OL]. IOP Conf. Ser. Earth Environ. Sci, 2012, 15(3): 32054. DOI: 10.1088/1755-1315/15/3/032054.

[2] novi yulia Budiarti. : volume 4[M/OL]. Sustain, 2020. https://pesquisa.bvsalud.org/portal/resource/en/mdl-20203177951%0Ahttp://dx.doi.org/10.1038/s41562-020-0887-9%0Ahttp://dx.doi.org/10.1038/s41562-020-0884-z%0Ahttps://doi.org/10.1080/13669877.2020.1758193%0Ahttp://sersc.org/journals/index.php/IJAST/article.

[3] Kosinska A, Balakin B V, Kosinski P. Theoretical analysis of erosion in elbows due to flows with nano- and micro-size particles[J/OL]. Powder Technol., 2020, 364: 484-493. DOI: 10.1016/j.powtec.2020.02.002.

[4] Zeng C, Xiao Y, Zhang J, et al. Numerical analysis of pelton turbine needle erosion characteristics[J/OL]. Journal of Drainage and Irrigation Machinery Engineering, 2015, 33(5): 407-411. https://www.researchgate.net/publication/282983395_Numerical_analysis_of_pelton_turbine_needle-_erosion_characteristics.

[5] Mazumder Q H, Zhao S, Ahmed K. Effect of bend radius on magnitude and location of erosion in s-bend[J/OL]. Model. Simul. Eng, 2015, 2015. DOI: 10.1155/2015/930497.

[6] al. R K. Effect of sand fines concentration on the erosion-corrosion mechanism of carbon steel 90o elbow pipe in slug flow[J/OL]. Materials (Basel)., 2020, 13(20): 1-16. DOI: 10.3390/ma13204601.

[7] Lospa A M, Dudu C, Ripeanu R G, et al. Cfd evaluation of sand erosion wear rate in pipe bends used in technological installations[J/OL]. in IOP Conference Series: Materials Science and Engineering, 2019, 514: 1. DOI: 10.1088/1757-899X/514/1/012009.

[8] Khan R, Ya H H, Pao W, et al. Erosion-corrosion of 30°, 60°, and 90° carbon steel elbows in a multiphase flow containing sand particles[J/OL]. Materials (Basel)., 2019, 12: 23. DOI: 10.3390/ma122333898.

[9] McLaury B S, Wang J, Shirazi S A, et al. Solid particle erosion in long radius elbows and straight pipes[J/OL]. Proceedings - SPE Annual Technical Conference and Exhibition, 1997: 977-986. DOI: 10.2523/38842-ms.

Appendix A.

Hydro Lab
IN COOPERATION WITH NTNU, NORWAY

HLPL/F/RSoLA/01

RESULT SHEET OF LABORATORY ANALYSES

Client:	Mr. Chiranjibi Acharya, Department of Mechanical and Aerospace Engineering, Pulchowk Campus, IOE, TU, Nepal		
Project:	Chameliya Hydropower Project		
Sampling location:	Project site		
Sample provided by:	Client		
Reporting date:	30 August 2022	Report no:	263-8.L1_rev1

Tests and number of analyses

SN	Types of Test		Qty	SN	Types of Test		Qty
A.	Drying & weighing of filter paper with sediment	√	10	B.	Particle size distribution (PSD)	√	5
C.	Mineral content	√	5	D.	Organic matters content	-	-

A. Results of dry weight of Suspended Sediment sample (filter paper sample)

S. No.	Sample No.	Sampling date	Dish no.	Dry wt. of filter paper with dish (gm)	Dry wt. of filter paper with sediment + dish (gm)	Net wt. of sample (gm)
1	7	03/05/2022	125	36.8476	37.2678	0.4202
2	8	13/05/2022	126	18.4374	18.9299	0.4925
3	4	23/05/2022	116	31.2356	32.8282	1.5926
4	3	03/06/2022	115	29.0467	31.5868	2.5401
5	10	13/06/2022	128	23.324	27.5863	4.2623
6	2	23/06/2022	114	31.0192	35.0647	4.0455
7	5	04/07/2022	117	30.9157	36.2244	5.3087
8	6	13/07/2022	124	28.935	32.9908	4.0558
9	9	23/07/2022	127	24.0798	26.4899	2.4101
10	1	02/08/2022	122	30.9195	32.9756	2.0561

Appendix B.

Hydro Lab
IN COOPERATION WITH NTNU, NORWAY

HLPL/F/RSoLA/01

B. Results of Particle Size Distribution (PSD)

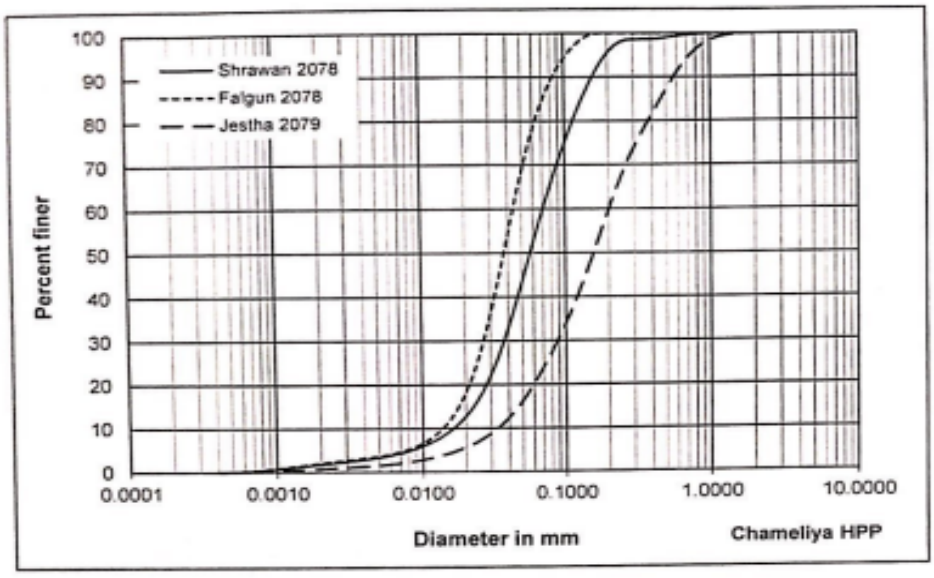

Figure B- 1: PSD curves of the suspended sediment samples taken on Shrawan 2078, Falgun 2078 and Jestha 2079

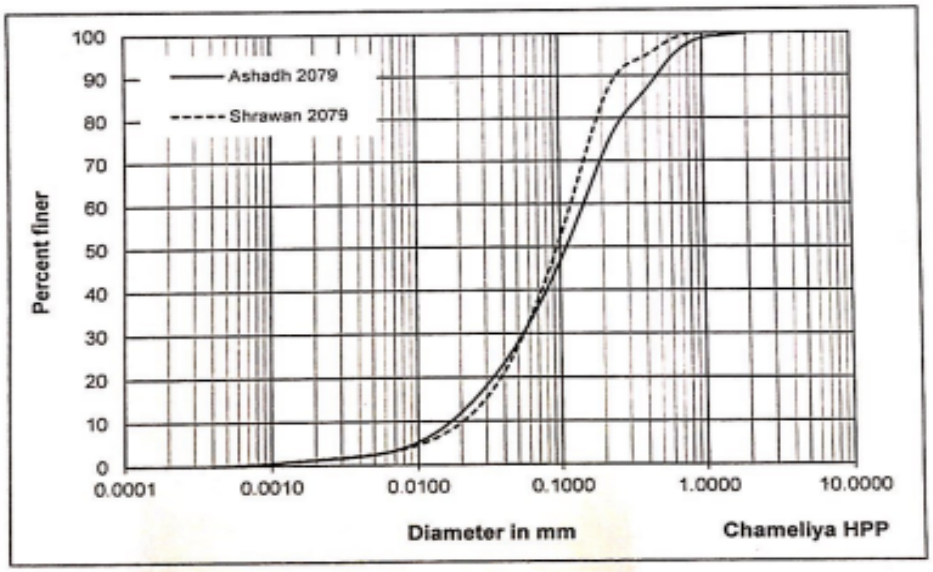

Figure B- 2: PSD curves of the suspended sediment samples taken on Ashadh 2079 and Shrawan 2079

HYDRO LAB PVT. LTD.

Appendix C.

Hydro Lab
IN COOPERATION WITH NTNU, NORWAY

HLPL/F/RSoLA/01

C. Results of Mineral Content

Table C-1: Shrawan 2078

Minerals		Sample (%)			Average (%)	Hardness (Moh's scale)
		1	2	3		
Quartz		65	69	67	67	7
Feldspar		2	3	1	2	6
Mica		16	13	16	15	2-3
Other	A	1	1	1	1	≥ 5
	B	16	14	15	15	< 5

Table C-2: Falgun 2078

Minerals		Sample (%)			Average (%)	Hardness (Moh's scale)
		1	2	3		
Quartz		68	64	66	66	7
Feldspar		3	2	4	3	6
Mica		14	15	13	14	2-3
Other	A	1	1	1	1	≥ 5
	B	14	18	16	16	< 5

Table C-3: Jestha 2079

Minerals		Sample (%)			Average (%)	Hardness (Moh's scale)
		1	2	3		
Quartz		70	68	69	69	7
Feldspar		2	2	2	2	6
Mica		11	15	13	13	2-3
Other	A	1	1	1	1	≥ 5
	B	16	14	15	15	< 5

Table C-4: Ashadh 2079

Minerals		Sample (%)			Average (%)	Hardness (Moh's scale)
		1	2	3		
Quartz		68	64	72	68	7
Feldspar		1	3	2	2	6
Mica		14	14	11	13	2-3
Other	A	1	1	1	1	≥ 5
	B	16	18	14	16	< 5

Table C-5: Shrawan 2079

Minerals		Sample (%)			Average (%)	Hardness (Moh's scale)
		1	2	3		
Quartz		68	67	69	68	7
Feldspar		2	2	2	2	6
Mica		12	15	12	13	2-3
Other	A	1	1	1	1	≥ 5
	B	17	15	16	16	< 5

Note:

Other A: Tourmaline, Garnet, hornblende and Olivine
Other B: Carbonate (~14 %), Clay, Organic matters, and up to 2% unidentified mineral and rock fragments (slate)

HYDRO LAB PVT. LTD. NEPAL